Wiley
International Journal of Energy Research
Volume 2025, Article ID 5398834, 18 pages
https://doi.org/10.1155/er/5398834

WILEY

Research Article

The Computational Modeling of Grid-Connected Double-Chamber Microbial Fuel Cell (DCMFC) Bioenergy Utilizing MATLAB Simulink Software

Khaya Pearlman Shabangu[1,2] **Nhlanhla Mthembu,**[2] **Manimagalay Chetty**[1,3] **and Babatunde Femi Bakare**[2]

[1] *Green Engineering Research Group, Department of Chemical Engineering, Faculty of Engineering and the Built Environment, Durban University of Technology, Steve Campus, S3 L3, P.O. Box 1334, Durban 4000, South Africa*
[2] *Environmental Pollution and Remediation Research Group, Department of Chemical Engineering, Faculty of Engineering, Mangosuthu University of Technology, P.O. Box 12363, Jacobs, Durban 4026, South Africa*
[3] *Department of Chemical Engineering, Faculty of Engineering and the Built Environment, Cape Peninsula University of Technology Symphony Way Belville, Cape Town, South Africa*

Correspondence should be addressed to Khaya Pearlman Shabangu; shabanguk@mut.ac.za; 20253160@dut4life.ac.za

Received 7 May 2024; Revised 29 October 2024; Accepted 4 January 2025

Academic Editor: Dr. Subhashree Choudhury

Owing to the depletion of fossil fuels, rising energy costs, and environmental pollution, there has been a growing focus on exploring and exploiting renewable energy sources. This study aims to demonstrate the modeling of a grid-connected double-chamber microbial fuel cell (DCMFC) biomass energy system via MATLAB Simulink software. The experimental measurements obtained from DCMFC outputs served as the basis for developing the inverter-grid connection model and simulation output in MATLAB Simulink software. Briefly, the DCMFC DC boost voltage was connected to the positive and negative buses of the three-phase DC–AC inverter circuit, with switching patterns controlled by gate pulses in each transistor. Full square wave single-stage PWM pulses are generated by the gate for control. The power generated by the inverter was measured via a three-phase VI block for analysis, with voltages and currents displayed via a scope. To address potential noise during switching, an LC filter is employed to suppress noise output and stabilize power generation. Another power meter measures power from the grid, with waveforms displayed via scope blocks. Before synchronization between power from the DCMFC and the grid occurs, four requirements must be met: the grid voltage must match the inverter output voltage, the inverter frequency must match the grid frequency, the phase sequence must be the same, and the phase angle of the inverter must match that of the grid. Additionally, Institute of Electrical and Electronics Engineers (IEEE)-specific requirements were evaluated during the simulation for this study. In addition, this study critically examined whether the DCMFC inverter model conforms to conventional requirements, International Electrotechnical Commission (IEC) standards, and IEEE standards for the integration of inverters into the grid. Compared with previous studies on inverter modeling for grid connections, past studies have emphasized the efficacy of biomass power plants and different inverter topologies for photovoltaic (PV) systems. The current study focuses on optimizing a multilevel inverter-based model, achieving low total harmonic distortion (THD) below IEEE standards. In this study, the use of a multilevel inverter configuration proved highly effective in reducing the harmonic content, leading to synchronized phase sequences and enhanced coherence between the grid and inverter voltages. With a THD of 4.75% at 50 Hz, supported by a harmonic distortion value of 422.5, the chosen configuration significantly minimized the harmonic distortion. This success underpins the system's reliability and efficiency, offering promising implications for practical applications.

Keywords: computational-modeling; DCMFC; grid-connection; IEC-standards; MATLAB-Simulink

1. Introduction

In recent years, the problem of energy in the country has increasingly been engraved, resulting in the implementation of load shedding to prevent the total collapse of the grid. Fossil resources worldwide have depleted rapidly as energy consumption has steadily increased, and the deregulation of electricity has caused the amount of installed production capacity of classical high-power stations to be unable to meet demand [1, 2]. This paper aims to demonstrate the modeling of a grid-connected double-chamber microbial fuel cell (DCMFC) biomass energy system via MATLAB Simulink software. The experimental measurements obtained from the DCMFC outputs serve as the basis for developing the model, which is simulated in MATLAB Simulink software. To encourage the use of renewable energy systems, some countries have initiated incentives to assist in alleviating the current energy crisis [1, 2]. Several studies have been conducted on renewable energy sources. Other studies [1, 2] used the honey well software to model 5 MW of biomass energy from wood waste in remote areas. The experimental data derived from the DCMFC outputs serve as the foundational basis for constructing the model, which is then simulated within the MATLAB Simulink environment. The simulated outcomes aim to provide insights into the potential power output that can be extracted from the DCMFC system, contributing valuable information to enhance energy production on the grid. This study not only delves into theoretical modeling but also involves practical considerations, utilizing real-world measurements to validate and inform the simulation process.

Furthermore, the investigation extends to assessing the DCMFC inverter's compliance with conventional requirements and Institute of Electrical and Electronics Engineers (IEEE) standards governing the integration of inverters into the power grid. This holistic examination ensures that the proposed DCMFC biomass energy system aligns with established industry standards, facilitating its seamless integration into existing grid infrastructures.

In grid-connected photovoltaic (PV) systems, inverters play a crucial role as power electronic converters, transforming DC power generated by solar panels into AC power compatible with the grid. There are three primary inverter topologies based on their architecture: the central inverter, the string/multistring inverter, and the module-integrated microinverter [1, 2]. The string inverter topology is a scaled-down version of the central inverter, where a certain number of modules are connected in series (string), and an inverter is linked to each string. In this configuration, each string operates with its own MPPT, enhancing the system's adaptability [1–7]. The multistring topology represents an evolution in the string inverter design, which is especially suitable for larger systems. Each string is equipped with its own DC–DC converter, and these strings are then linked to a common inverter, optimizing efficiency and performance [3–8].

The imperative for advancing renewable energy has intensified globally as nations endeavor to diminish their reliance on fossil-derived sources. In Africa, biomass constitutes a substantial portion of renewable energy, although its utilization remains largely rudimentary, primarily for cooking and heating. Such primitive applications not only underutilize the true energy potential of biomass but also contribute to premature mortality due to pollution [9–15]. In South Africa, challenges such as a limited water supply and infrastructure tailored to coal-based energy production have impeded the progression of bioenergy [9]. The stated policy scenario has delineated energy targets for South Africa to reach by 2040, aiming to optimize the utilization of available biomass [9, 10, 14, 16–20]. To assess the feasibility of these goals, data on biomass quantities for diverse types have been acquired, scrutinizing the availability of biomass for energy generation [9].

Various biomass conversion technologies have been explored to compare their efficiency and production costs, facilitating an analysis of the most suitable technology for application in South Africa [9, 21]. Scenarios have been formulated, incorporating insights from prior research and interviews to influence the selection of biomass conversion technology and identify the most promising end products [9, 21–23]. Given the adoption of DCMFC technology, this study suggests that bioenergy could replace up to 15% of coal-based energy production in South Africa [9, 18, 24–26] with competitive pricing relative to current electricity and fuel rates. However, this transition necessitates political backing, public trust, and substantial investment. Increased bioenergy adoption not only diminishes the dependence on fossil fuels but also optimizes the utilization of available renewable resources, thereby increasing energy security [9, 21–23, 27]. Moreover, a more efficient bioenergy utilization model would mitigate premature deaths resulting from the primitive use of biomass, reduce emissions, and foster a healthier environment.

In essence, this research endeavors to bridge the gap between theoretical modeling and practical implementation by leveraging MATLAB Simulink for simulation purposes. The focus on compliance with industry standards enhances the study's relevance, making it a comprehensive exploration of the viability of DCMFC biomass energy systems as sustainable and grid-compatible renewable energy sources. The inclusion of a grid-connected aspect suggests a focus on integrating the DCMFC bioenergy system into an existing power grid. This involves studying the interaction between the DCMFC system and the grid, exploring possibilities for energy exchange, and addressing challenges related to grid integration. The specific emphasis on DCMFCs indicates a unique approach to microbial fuel cell (MFC) technology. The double-chamber design may have novel features or advantages over traditional MFCs; hence, the purpose of this study is to delve into the intricacies of its operation and performance towards computational scaling up of bioelectricity production with the integration of an inverter model to mimic the practicality and applicability of this study for grid connection prospects.

The use of MFCs for bioenergy production is an established field [1–3], but the specific application of DCMFC for bioenergy generation suggests an advancement or refinement in the technology [1–3]. This study explores efficiency improvements, scalability, or other enhancements in bioenergy production compared with those of conventional MFCs. The utilization of MATLAB Simulink for modeling implies a sophisticated and detailed simulation approach [1–3]. This choice of software suggests a focus on accurate and dynamic modeling, enabling the study of the DCMFC system under various conditions and scenarios [1–7, 9–19]. The emphasis on modeling indicates a theoretical exploration of the DCMFC system, likely involving mathematical representations and simulations. This knowledge will contribute to a deeper understanding of DCMFC system behavior, performance optimization, and possibly the development of control strategies for practical implementation and application as a local South African national grid connection alternative reliable energy source next to solar power and other alternatives [19–24].

Solar PV energy has become a significant focus for researchers due to its rapid global adoption [2–28]. Despite its numerous advantages, PV energy poses certain challenges, particularly concerning power factor (PF) and total harmonic distortion (THD) [28]. When integrated into the grid, solar PV systems can lead to various power quality issues. These issues, such as component overheating and suboptimal operation, arise mainly from low power quality and high harmonics, causing significant damage. The magnitudes of PF and THD are influenced by solar irradiation levels [28]. This article examined how changes in solar irradiation (G) impact power quality in grid-connected solar systems, presenting and analyzing results for different irradiation conditions [28]. At low irradiance levels, the amplitude of harmonic components and reactive power increases while the PF decreases, leading to reduced system efficiency. This study measured PF and THD for current (THD_I) values on a particularly cloudy day to conduct an analysis [28]. Using MATLAB for simulation, a grid-connected PV system model was developed [28]. The relationship between PF, THD_I, and solar irradiation was analyzed using the Statistical Package for the Social Sciences (SPSS) program and the curve fitting method. The study derived new analytical expressions for PF and THD_I based on irradiation levels. These expressions can mitigate low power quality issues in low solar irradiation scenarios, offering a valuable contribution to the existing literature [28–30].

The current study builds on the innovative work of Adak and Cangi [28–33] by developing an integrated grid-connected operation of a DCMFC bioenergy system through advanced modeling techniques using MATLAB Simulink. Emphasizing the double-chamber design integrated with a multilevel inverter in a three-phase, 400 V system, this study introduces the novel concept of an integrated DCMFC for consideration as an alternative sustainable and renewable power source, particularly beneficial for power-starved and crisis-engulfed nations like South Africa. This research makes a significant contribution to the field of bioelectricity grid-connected power systems using DCMFC technology. The following flowchart provides a clear summary of the novel methodological approach used to computationally model and simulate the proposed practical and applicable DCMFC integrated prototype in MATLAB Simulink. This study examines and contributes new knowledge of whether the DCMFC-inverter integration conforms to IEEE standards for grid synchronization to the existing prospects of DCMFC grid connection.

2. Materials and Methods

This section describes the approach strategy and approach that was adopted in the simulation and optimization of the laboratory experimental data obtained in the treatment of both biorefinery and dairy wastewater streams that were used as complex wastewater substrates and biofuel sources for the bioelectrochemical production of power in a DCMFC. The flowchart in Figure 1 and the process block diagram in Figure 2 outlines the process of integrating the MFC into a grid. Initially, the MFC generates electricity through a bioelectrochemical reaction between the anode and cathode terminals, reaching a peak of 700 mV, as indicated in the sections below. The detailed experimental data are presented downstream with the accompanying bioelectrochemical parameters used to classify DCMFC treatment efficacy. The DCMFC cells are then interconnected in series to achieve a 12 V voltage level suitable for standard inverters. The research focuses on integrating a 12 V DCMFC sustainable bioelectricity supply to a 400 VAC inverter.

The DCMFC battery supply is first assessed for voltage levels. If the voltage deviates from the specified threshold, protection circuits are activated to safeguard and disconnect the inverter from the grid. If the voltage is within the acceptable range, it is stepped up to 400 VDC using DC–DC converter circuitry. Once the grid voltage and frequency are at 400 VAC/50 Hz, the 400 VDC is converted to AC by a three-phase bridge circuit with a phase angle of 120°. If the voltage, frequency, or phase angle does not align with grid specifications, the protection mechanism isolates the inverter from the grid. The inverter remains synchronized with the grid as long as voltage, frequency, phase angle, and sequence correspond with grid standards.

The DCMFC battery output is connected to a DC–DC conversion block. The voltage fluctuates based on microbial activity within the DCMFC chamber, so a DC–DC boost converter is employed to maintain a stable output for the inverter. The inverter block transforms the power into an AC output suitable for AC loads and the grid. Similarly, solar energy harnessed during the day using PV panels generates DC power that is fed into the DC–DC block. The DC input is stepped up to share the connection with the DCMFC at the DC bus. Before synchronizing the inverter's power with the grid, criteria including voltage, frequency, phase angle, and phase sequence must be met.

2.1. Standards of Inverter Grid-Connected Systems. To increase the reliability of the system, adherence to the standards set by the International Electrotechnical Commission (IEC) and the IEEE is imperative for connecting the inverter to the grid. The primary objective of the inverter is to deliver a sinusoidal current to the grid. As renewable energy systems rapidly evolve, standards governing inverter-grid connections are continuously evolving, guided by national and

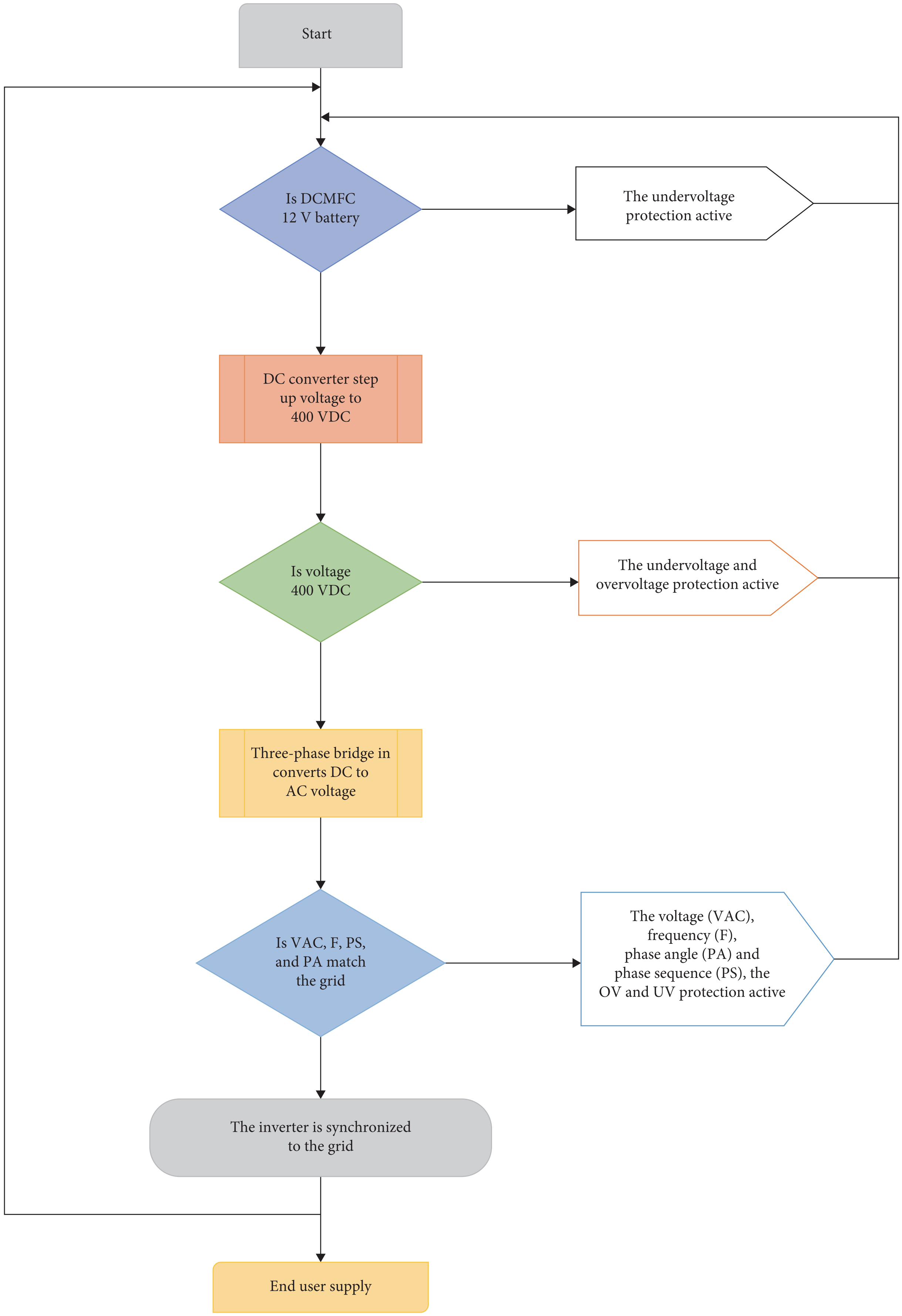

Figure 1: Flowchart for a novel DCMFC integration into a grid connection. DCMFC, double-chamber microbial fuel cell.

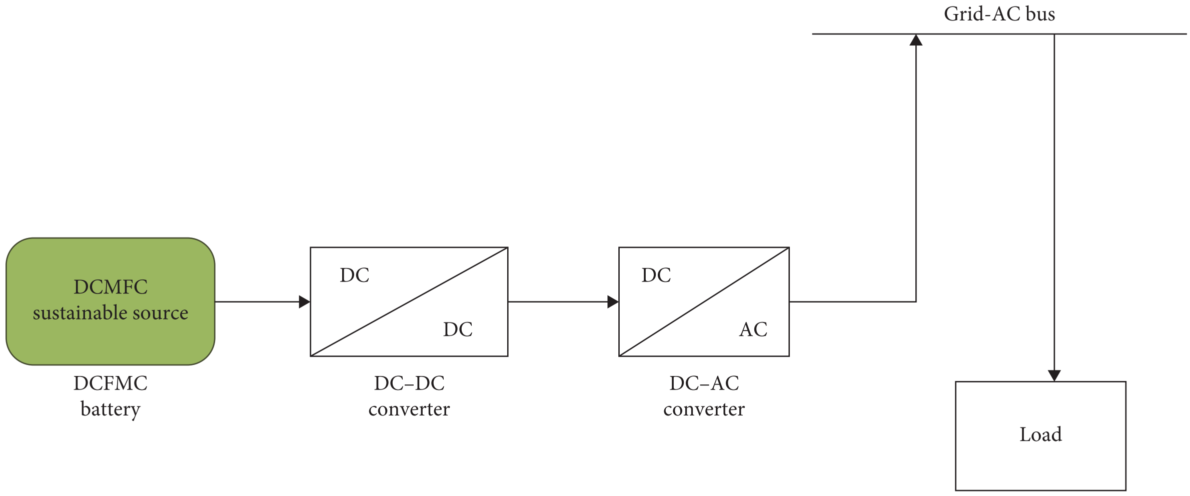

Figure 2: Block diagram for the grid-connected-DCMFC for bioenergy production. DCMFC, double-chamber microbial fuel cell.

international committees such as the IEC and IEEE. The connection of PV systems to the grid through inverters necessitates strict compliance with terms outlined in standards. These include but are not limited to THD, DC current injection, galvanic isolation, anti-islanding detection, and adherence to specified voltage and frequency ranges for uninterrupted operation. These parameters are critical for ensuring the seamless integration of PV systems into the grid, and their compliance is defined by established standards [34].

2.1.1. THD. In accordance with the stipulations outlined in the IEEE 1547 and IEC 61727 standards, THD should not exceed 5%, and efforts should be made to minimize the harmonic content of the injected current. These standards also impose restrictions on DC current injection, with a maximum limit of 1% per IEC 61727 [5] and a more stringent limit of 0.5% according to IEEE 1547 standards [35]. To mitigate THD in the injected current, the implementation of soft computing methods proves instrumental in refining the switching modulation technique employed by the inverter. This strategic integration of soft computing techniques contributes to the enhancement of inverter performance, aligning with the stringent standards set forth by the IEEE and IEC [36].

2.1.1.1. THD Formulas. THD is a measure of the distortion of a signal due to harmonics [32, 33, 36]. It is defined for both current and voltage as follows:

THD for voltage: The THD for voltage (THD_V) is calculated using the root mean square (RMS) values of the harmonics of the voltage signal. It is given by [32, 33, 36]:

$$THD_V = \sqrt{\frac{V_2^2 + V_3^2 + V_4^2 + \ldots + V_n^2}{V_1}} \times 100\%, \quad (1)$$

where

- V_1 is the RMS value of the fundamental voltage component.
- V_2, V_3, V_4…. Vn are the RMS values of the 2nd, 3rd, 4th, …, nth harmonic components of the voltage.

THD for current: The THD_I is similarly calculated using the RMS values of the harmonics of the current signal. It is given by [32, 33, 36]:

$$THD_I = \sqrt{\frac{I_2^2 + I_3^2 + I_4^2 + \ldots + I_n^2}{I_1}} \times 100\%, \quad (2)$$

where

- I_1 is the RMS value of the fundamental current component.
- I_2, I_3, I_4…. In are the RMS values of the 2nd, 3rd, 4th, …, nth harmonic components of the current.

These formulas help in quantifying the extent of harmonic distortion in voltage and current signals, which is crucial for assessing power quality in electrical systems.

2.1.2. Anti-Islanding Detection. The significance of anti-islanding detection lies in its crucial role in promptly discontinuing the injection of power into the grid by the inverter in the event of a fault on the grid side. The occurrence of islanding poses hazardous effects on the equipment within the system, underscoring the imperative need for robust anti-islanding detection mechanisms. In accordance with the rigorous criteria established by the IEEE 1547 and IEC 61727 standards, some authors [36] distributed generation inverter systems are mandated to swiftly identify and isolate islanding conditions within a stringent timeframe of 2 s [36]. Various methodologies are employed for the detection of islanding conditions, ensuring compliance with the stipulated standards [37]. This stringent approach not only aligns with regulatory requirements but also safeguards the integrity and reliability of the overall grid-connected system.

Table 1: DC–DC converter measurement results.

Voltage input	Voltage input (V)	Voltage output (V)
Modeling results	12.0	400
Simulation results	12.0	400
Experimental results	12.4	400

2.1.3. Galvanic Isolation. In accordance with the National Electrical Code (NEC), the implementation of galvanic isolation is mandated for inverter-based energy systems operating at voltages exceeding 50 V. Galvanic isolation has a distinct advantage in such systems, as it ensures that faults occurring on one side of the grid-connected system do not adversely affect the other side [34, 35, 37, 38]. Galvanic isolation is a technique that physically separates electrical circuits to prevent direct current flow between them [39]. This separation not only serves to increase safety by mitigating the risk of electric shock but also plays a crucial role in preventing the propagation of faults. In grid-connected systems, where stability and reliability are paramount, galvanic isolation acts as a protective barrier, isolating potential issues and containing their impact within the affected circuit [36]. This proactive approach aligns with safety standards and contributes to the robustness of inverter-based energy systems, especially when voltages surpass the designated threshold outlined by the NEC [34, 35, 37, 38, 40].

2.1.4. DCMFC-Inverter Prototype

2.1.4.1. DC–DC Step-Up Converter. Following a series of simulations conducted using various electrical software applications, the Proteus software appeared to yield responses consistent with the model and outcomes derived from MATLAB software. The objective was to ascertain the appropriate component values that would be suitable for the experimental prototype of the integration of DCMFC into a power grid. During the simulation from Proteus software, the 12 V from the DCMFC battery was increased to 400 V as it was with the MATLAB model. Table 1 of the simulation, MATLAB model, and measurement results is given below.

From the Proteus software simulations, the specifications of electrical components were established. On the picture in Figure 3 are some of the pictures taken during the testing of the DCMFC DC–DC converter circuit. The pictures show the power supply, microcontroller with LCD display, MOSFET circuit, and Fluke digital multimeter. The adjustable power supply acts as a source in the circuit, which represents the MFC battery behavior. The power supply used in the experiment was selected due to its capability to adjust voltage or current or both, which is favorable to the DCMFC cell and battery as per the model from MATLAB software. During the testing, it was observed the DC voltage changing from 12 to 400 V.

2.1.4.2. Three-Phase Inverter Bridge. From the DC–DC converter, the 400 VDC power is connected across the three-phase bridge bus terminals. The pulses and the sequencing of the three-phase bridge are controlled by a microcontroller, as shown in the pictures of Figure 3. The RC load was used between the three-phase bridge and the grid supply.

2.1.4.3. The Synchronization of MFC Battery Into a Grid. According to IEEE standards the requirements that must met before the synchronization of the inverter into a grid are namely: the frequency of the grid must equal to the inverter output, the line voltage must be equal, the phase sequence must be of the same rotation, the phase angle must be equal. Although the prototype was not synchronized to do availability of the synchronizing meters, the grid bus and inverter bus were able to generate the voltage equal to the grid, as shown in Figure 4 and Table 2.

2.1.5. Bioelectrochemical Analysis of Biorefinery and Dairy Wastewater in DCMFC-Based Optimal Bioelectricity Validation Experiments

2.1.5.1. Real-Time Experimental Set-Up for the DCMFC Bioelectricity Optimization Process: DCMFC Experimental Configuration. The MFC chamber utilized in this study is a dual-chamber design fabricated from two Schutt blue cap 1 L bottles. The anode and cathode chambers were separated by a Nafion 115 proton exchange membrane (PEM) (Lyntech, United States), which facilitates the transfer of protons (H^+) from the anode chamber to the cathode chamber. Copper-bi-electrodes augmented with carbon-graphite were selected as the electrodes and positioned in both the anode and cathode chambers, with a cross-sectional area of 0.237 m^2. The bi-electrode connection was completed by an external circuit using professional electrical positive and negative wires to transfer electrons produced from the oxidation of organic matter from the anode chamber to the cathode chamber.

An external load of 1000 Ω is commonly set as a reference standard operating threshold to enhance bacterial activity rates, as demonstrated by Logan et al. [34, 39–49] and other authors [2, 11–15], who clearly articulate the methodology and efficient experimental setup required to attain practical results in a typical MFC system. Based on these findings, this study adopted a higher operating external resistive load capacity of 1300 Ω. This adjustment aligns with the bioelectrochemical principle stated by Zhang et al. [50, 51], which indicates that MFCs with reduced external resistance during startup exhibit elevated rates of energy gain, energy output, active biomass, and maximum power density, although the rate of voltage increase decreases [50, 51].

The cathode compartment was filled with a standard 0.1N potassium permanganate solution combined with slow oxygen sparging as electron acceptors, Shabangu et al. [52]. Figures 5 and 6 illustrate the startup experimental process flow diagram and the laboratory view images of the DCMFC with its distinctive components utilized during the startup experimental runs. Following the operational sequence adopted from Logan et al. [34, 39–49] and other referenced studies, this unit was primarily operated at 1300 Ω at startup and maintained this setting throughout the experimental runs.

A critical part of the objective calibration sequence was observing the effect of temperature on the overall resistivity

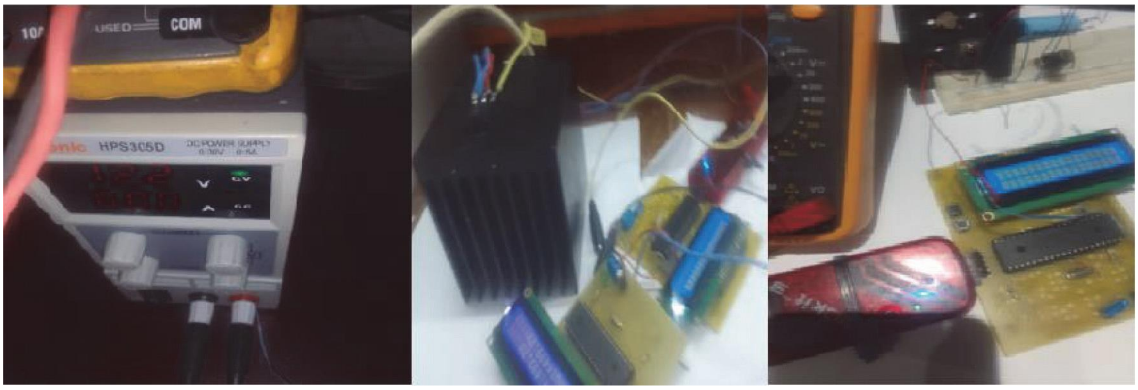

Figure 3: PCB prototype for the DCMFC-inverter integrated system. DCMFC, double-chamber microbial fuel cell.

Figure 4: Grid-connection lab prototype layout.

Table 2: Three-phase inverter measurements.

Voltage input	DC bus voltage (V)	H-bridge AC voltage (V)
Modeling results	400	400
Simulation results	400	400
Experimental results	400	400

of the unit. Different temperature gradients resulted in varying resistance loads at specific percentage openings. Figure 5 presents the behavioral sequence of the resistance box at 18, 22, and 34.5°C, underscoring the importance of the calibration curve in determining the desired percentage load opening at specific temperatures through extrapolation from the presented calibration curve measurements. The content of the calibration sequence prior to each fed-batch was sourced from the content of published work on the DCMFC start-up sequence and calibration of cell chambers by Shabangu et al. [53].

2.1.5.2. Inoculation and Medium. Raw industrial wastewater, characterized by high organic content (COD: 250–1850 mg/L for biorefinery wastewater and 500–3500 mg/L for dairy wastewater, with pH 6–7 for both streams), was sourced from local wastewater treatment plants (Tongaat Hulett, Rossburgh, and Clover Pty Ltd, Queensburgh, South Africa). Active microbial communities, specifically Proteobacteria and Bacteriodota, were also collected alongside the fresh industrial wastewater streams to serve as electrogens for the bioelectrochemical process. The objective was to enhance the biodegradation of complex substrate pollutants in these wastewater streams while generating bioelectricity, as reported by Shabangu et al. [53].

Dairy and biorefinery wastewaters were blended to mimic realistic downstream conditions, where effluent streams from various chemical plants and manufacturing operations are combined for further treatment in municipal sewer systems. These streams, characterized by complex substrates with high molecular energy potential, serve as reliable and enduring electron donors or anolytes for MFCs, contributing to bioelectricity production [2–10, 15].

According to Shabangu et al. [52], to ensure simplicity and reproducibility, the experimental procedures involved mixing 50% by volume (*v/v*) of each wastewater sample from dairy and biorefinery sources in a 1 L beaker. This mixture was allowed to blend slowly for 24 h at mesophilic temperatures [9, 10, 17]. This process was conducted immediately using onsite samples from the nearby wastewater treatment facilities. The pH was not controlled, allowing it to reflect the natural buffering capacity of the combined streams in downstream municipal receiving bodies, thus simulating natural environmental conditions.

2.1.5.3. DCMFC Data Analysis. The real-time performance monitoring data for the DCMFC unit was captured and

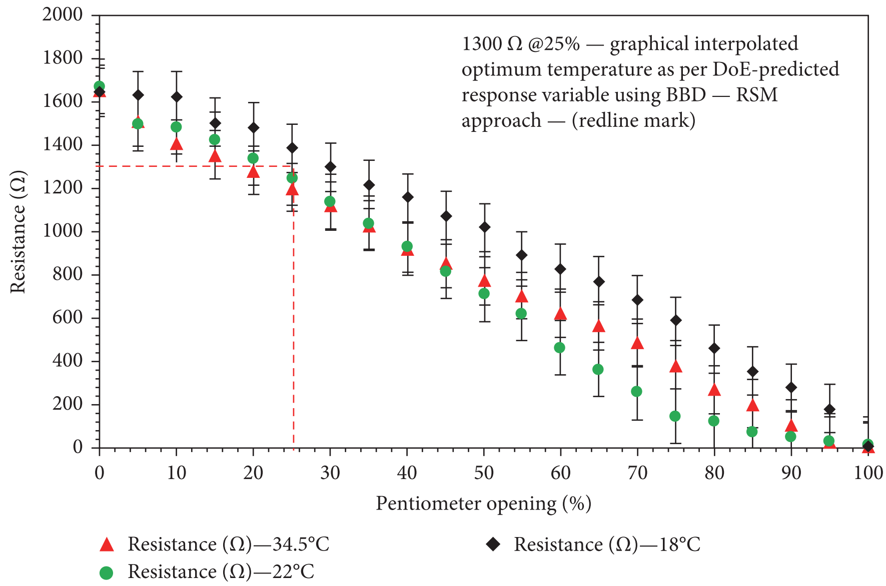

Figure 5: Resistance calibration test at 18, 22, and 34.5°C, Shabangu et al. [52, 53].

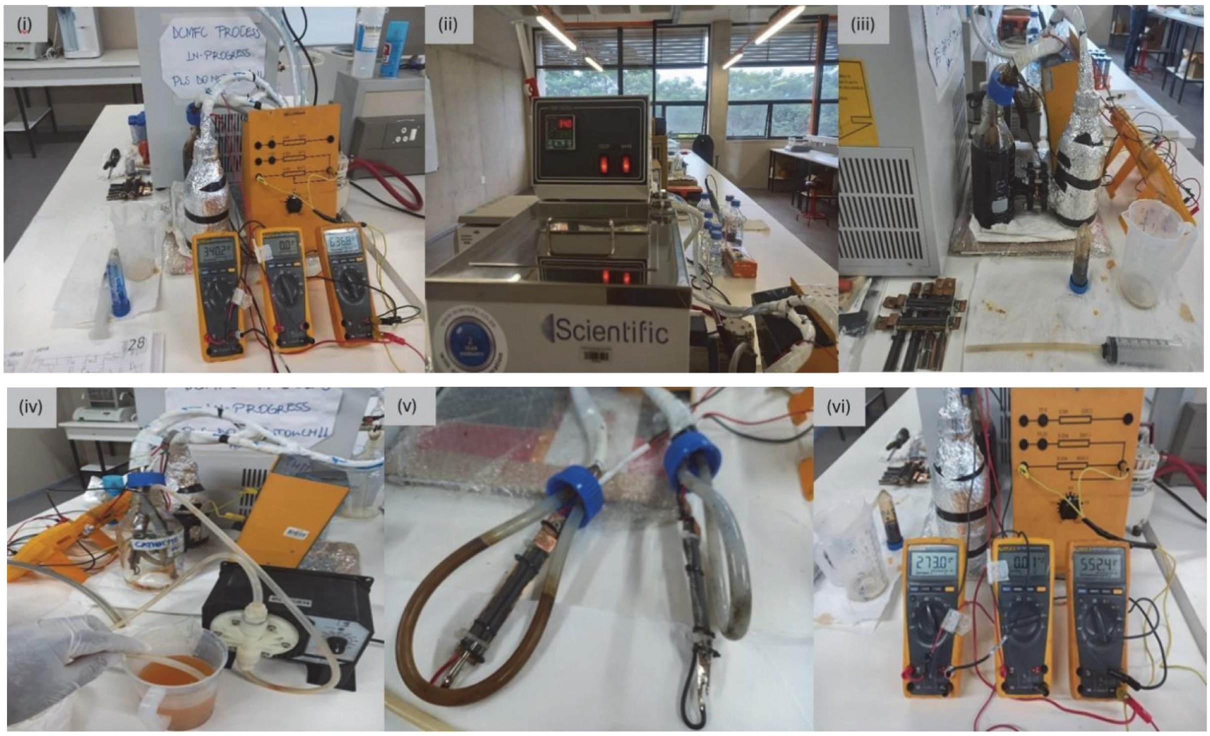

Figure 6: Real-time experimental set-up for the DCMFC, Shabangu et al. [52, 53]: (i) lab-set-up for the DCMFC in real-time, (ii) thermo-controller for controlled mesophilic–pyscrophylic temperature, (iii) side view showing the cathodic medium and 0.1N as per optimized response output by the BBD–RSM design, (iv) the real-time fed-batch stop and subsequent start-up, (v) view the CCu-bi-electrode configuration with water circulating manifolds, and (vi) real-time optimized runs CCV values for the DCMFC. DCMFC, double-chamber microbial fuel cell; RSM, response surface methodology.

calculated using established electrochemical models and expressions, as reported by Logan et al. [18–21] and Shabangu et al. [52, 53]. Electrical current (I) and voltage (V) measurements were taken using a multimeter every 5 h over a precise 48-h optimum incubation period [18].

$$I(\text{mA}) = \frac{V}{R_{\text{ext}}}, \quad (3)$$

where R_{ext} was the resistance of an external resistor that value was equal to $1000\,\Omega$ V (mV) is the voltage capacity, closed circuit voltage of the MFC unit.

$$\Delta G_r(\mathrm{J}) = \Delta G_r^0 + RT\ln(\pi), \tag{4}$$

where $\Delta G_r(\mathrm{J})$ is Gibbs free energy for specific conditions, ΔG_r^0 (J) is the Gibbs free energy under standard conditions usually defined by 298.15 K, 1 bar-pressure, and 1 M concentration for all species, R (8.31447 $\frac{J}{\mathrm{molK}}$) is the basic universal gas constant, T (K) is the absolute temperature calculated as the activities of the products divided by those reactants. The standard Gibbs free energy is calculated from tabulated energies of formation for organic compounds in water, sources available from Shabangu et al. [52, 53].

$$E_{\mathrm{emf}}(\mathrm{mV}) = -\frac{\Delta G_r}{nF}, \tag{5}$$

where all biodegradation reactions transpire under standard conditions; hence, $\pi = 1$, then equation simplifies further, sourced from Shabangu et al. [52].

$$E^0_{\mathrm{emf}}(\mathrm{mV}) = -\frac{\Delta G_r^0}{nF}, \tag{6}$$

$$P(\mathrm{mW}) = IE_{\mathrm{cell}}, \tag{7}$$

where $P(\mathrm{mW})$ is the overall power of the MFC unit. Normally, the voltage is measured across a fixed external resistor (R_{ext}, while the current is calculated from Ohms law: $I(\mathrm{mA}) = \frac{E_{\mathrm{cell}}}{R_{\mathrm{ext}}}$. By Logan et al. [43]:

$$\varepsilon_{Cb}(\%) = \frac{M\int_0^{t_b} Idt}{FbV_{\mathrm{Anode}}\Delta\mathrm{COD}}, \tag{8}$$

where $M = 32$ (molecular weight of oxygen), F is Faraday's constant, $b = 4$ (the number of electrons exchanged per mole of oxygen), V_{Anode} is the volume of the anodic chamber, and ΔCOD (mgCOD/L) is the change in COD over time t_b, as sourced from Logan et al. [18]. The empirical models and equations used for bio-electrochemical calculations in the startup of the DCMFC for electricity generation in this manuscript were sourced from Shabangu et al. [34, 35, 37, 38, 40, 43, 52, 53] and Logan et al. [34, 39–49].

Table 3 meticulously present a comprehensive bioelectrochemical analysis of two distinct wastewater streams: the optimized industrial wastewater streams and the mixed wastewater streams derived from biorefinery processes. These streams have been strategically chosen as the most effective electron donors or complex organic substrates, following an extensive validation process conducted experimentally over a span of 2 weeks. The experimental validation process employed rigorous scaling-up factors derived from the optimal operating conditions, which were determined through the application of design expertise utilizing response surface methodology (RSM), specifically employing the Box–Behnken design quadratic modeling sequence sourced from Shabangu et al. [52, 53]. The culmination of this process is reflected in Tables 1 and 2, where the achieved optimum laboratory experimental voltage yields are explicitly outlined. These voltage yields, ranging from 550 to 700 mV, underscore the efficacy of the chosen electron donors and organic substrates within the specified experimental parameters [34, 37, 40, 43, 52, 53].

3. Results and Discussions

3.1. The Modeling DCFMC Battery Grid-Connected Design Model. The DCMFC battery grid-connected design model represents an innovative approach to sustainable energy generation and storage. In this context, the DCMFC, which is a type of MFC, is integrated into a grid-connected system to harness, store, and supply electrical energy. The DCMFC operates on the principle of microbial electrochemical processes, where microorganisms generate electricity through the oxidation of organic matter [34, 39, 43–49]. The double-chamber design allows for controlled microbial reactions, enhancing the efficiency of the energy conversion process [54–56].

In the grid-connected design model, the DCMFC serves as a unique bioenergy source that can contribute to the overall power supply of the electrical grid. The model involves the development of a comprehensive mathematical and computational representation MATLAB Simulink. This representation considers the dynamic interactions within the DCMFC system and its connection to the grid. The primary goals of this design model include predicting the power output from the DCMFC, understanding the system's behavior under different conditions, and ensuring seamless integration with the grid. The integration involves the use of appropriate converters, inverters, and control systems to regulate the flow of electricity between the DCMFC and the grid. Figure 7 outlines the DCMFC battery inverter integrated grid-connected MATLAB model.

The DCMFC DC boost voltage is connected to the positive bus and negative bus of the three-phase DC–AC inverter circuit. The switching pattern is controlled by the gate pulses connected in each transistor of the inverter circuit. The pulses generated by the gate are full square wave single-stage PWMs. The power generated by the inverter is fed to the three-phase VI block for measurements. For analysis, the voltages and currents are displayed using the scope shown in Figure 7. While the noise may be generated from the DC to AC transition, the LC filter is employed to suppress the noise output and stabilize the power generated by the inverter. The second power meter is connected to measure the power from the grid. For each power meter, the waveforms are displayed via scope blocks. Before power from the DCMFC and grid are synchronized, four requirements must be met. First, the voltage of the grid must be equal to the inverter output voltage. Second, the inverter frequency must match the frequency of the grid. Third, the phase sequence must be the same. Fourth, the phase angle of the inverter must be equal to the grid. In addition, Tables 4 and 5 present the IEEE-specific requirements data for connecting inverters

Table 3: DCMFC measurement results from the biorefinery wastewater stream Shabangu et al. [52, 53].

				Optimized experimental runs for the treatment of biorefinery WWT source							
HRT (h)	**CCV load (mV)**	**Anode electrode (mV)**	**Cathode electrode (mV)**	E^{o}_{emf} **(mV)**	G_r **(J)**	**Columbic efficiency (%)**	**Current (mA)**	**Current density (mA)/m^2**	**Power (mW)**	***P* (cathode) (mW/cm^3)**	**P (anode) (mW/cm^2)**
0	390.4	290.7	100.4	391.1	−3.77E + 07	0.00	0.3904	30.3577	152.41	0.1524	22.9364
5	454.6	291.4	110.2	401.6	−3.87E + 07	14.89	0.4546	35.3499	206.66	0.2067	31.1002
10	559.2	287	238.4	525.4	−5.07E + 07	18.31	0.5592	43.4837	312.70	0.3127	47.0586
15	562.4	273.9	263.4	537.3	−5.18E + 07	18.42	0.5624	43.7325	316.29	0.3163	47.5988
20	575.1	285.5	242.3	527.8	−5.09E + 07	18.83	0.5751	44.7201	330.74	0.3307	49.7728
24	659.3	306.2	265.2	571.4	−5.51E + 07	21.59	0.6593	51.2675	434.68	0.4347	65.4141
30	700	348	298.3	646.3	−6.24E + 07	22.92	0.7000	54.4323	490.00	0.4900	73.7397
35	700	356.7	299.4	656.1	−6.33E + 07	22.92	0.7000	54.4323	490.00	0.4900	73.7397
40	648.2	334.8	289.3	624.1	−6.02E + 07	21.23	0.6482	50.4044	420.16	0.4202	63.2300
48	646.2	385	277	662	−6.39E + 07	21.16	0.6462	50.2488	417.57	0.4176	62.8404

Abbreviation: DCMFC, double-chamber microbial fuel cell.

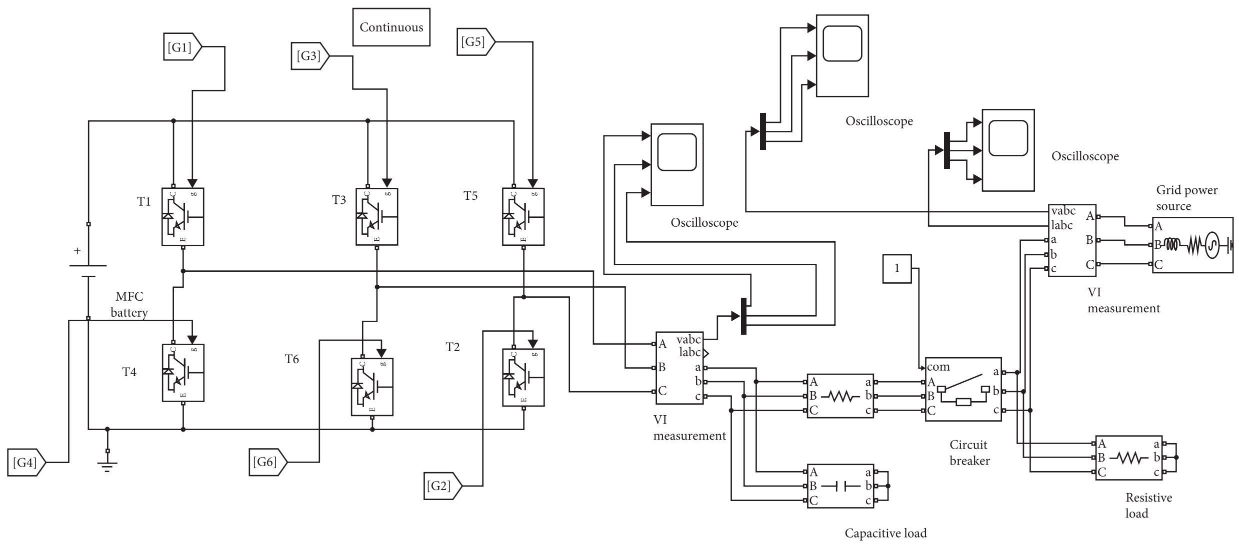

FIGURE 7: DCMFC-inverter model prototype for grid connection. DCMFC, double-chamber microbial fuel cell.

TABLE 4: Voltage distortion limits [44].

Bus voltage V at PCC	Individual harmonic (%) $h \leq 50$	THD (%)
$V \leq 1.0$ kV	5.0	8.0
1 kV $\leq V \leq$ 69 kV	3.0	5.0
69 kV $\leq V \leq$ 161 kV	1.5	2.5
161 kV $\leq V$	1.0	1.5[a]

Abbreviation: THD, total harmonic distortion.
[a]Indicates the frequency-dependent consideration—the harmonic distortion analyses consider different orders depending on system characteristics (e.g., low- or high-voltage).

TABLE 5: Current distortion limits for systems rated 120 V through 69 kV [44].

	Maximum harmonic current distortion in percent of I_L					
	Individual harmonic order[b]					
I_{SC}/I_L	$2 \leq h$ 11[a]	$11 < h \leq 17$	$17 \leq h < 23$	$23 \leq h < 35$	$35 \leq h \leq 50$	TDD
<20°	4.0	2.0	1.5	0.6	0.3	5.0
20 < 50	7.0	3.5	2.5	1.0	0.5	8.0
50 < 100	10.0	4.5	4.0	1.5	0.7	12.0
100 < 1000	12.0	5.5	5.0	2.0	1.0	15.0
>1000	15.0	7.0	6.0	2.5	1.4	20.0

[a,b]Indicate the frequency-dependent consideration—the harmonic distortion analyses consider different orders depending on system characteristics (e.g., low- or high-voltage).

into a grid, which will be evaluated for this study during the simulation.

3.2. DCMFC Simulation Results. Figure 8 illustrates a sinusoidal pattern that shows three-phase voltages recorded at 400 V and 50 Hz before synchronization with the grid. This study specifically opted for a multilevel inverter configuration, which was chosen for its ability to reduce the harmonic content effectively [43]. The three-phase waveforms are distinctly separated at 120° intervals, maintaining a synchronized and visually distinguishable phase sequence represented in red, yellow, and blue throughout the simulation, as shown in Figures 9 and 10, is accompanied by a comprehensive caption that integrates both the grid voltage and the inverter voltage. The visual representation in the caption underscores the coherence between the grid and inverter voltages.

In the subsequent caption, the calculated THD is meticulously measured, yielding a fundamental capacity of 4.75% at a frequency of 50 Hz. This finding is visually depicted in Figure 11, where the harmonic distortion is quantified at 422.5. The adoption of the multilevel inverter configuration in this study proves instrumental in achieving reduced harmonic content, as evidenced by the low THD values observed in the simulation results.

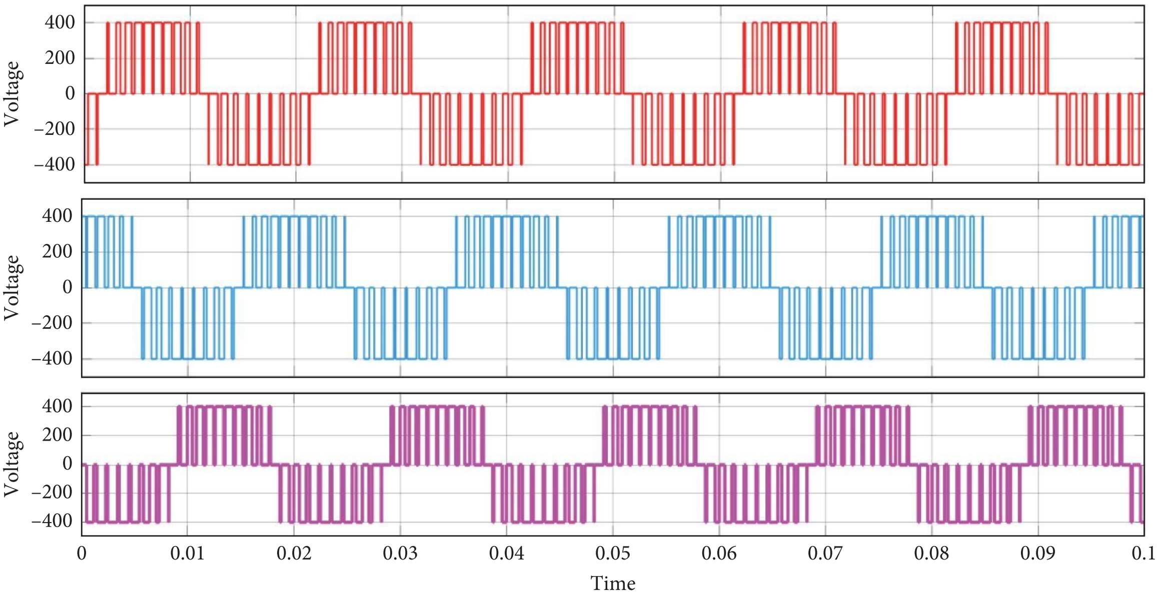

FIGURE 8: DCMFC inverter output waveform before synchronization. DCMFC, double-chamber microbial fuel cell.

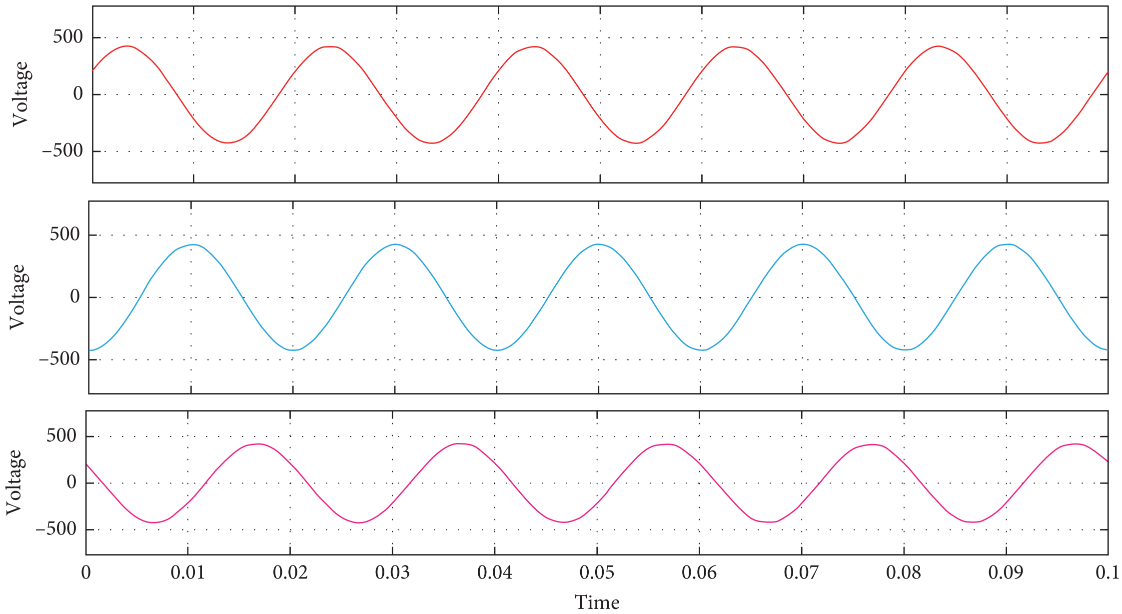

FIGURE 9: Grid AC-voltage before synchronization.

3.3. Comparative Analysis of Inverter Model Standards and Performance Fundamental for Grid-Connection Limitations. Table 6 presents a summary of the previous work on inverter modeling for practical grid connection in comparison with the current study outcomes. The Honeywell model for biomass power plants reported by Norder et al. [36, 57] highlights the main components of this model, with the boiler, steam turbine, and generator being crucial for producing a 5 MW overall power output. Henceforth, for the purposes of upscaling, ~8.33 tonnes/h of wood waste is imperative to maintain a threshold power of 5 MW [36, 57]. The Honeywell model is based on the following system parameters for power generation model simulation: temperature, pressure, and overall steam plant mass flowrate capacities (tonnes/h). The process simulation and cost optimization sequence for the Honeywell model, which is based on a solar and biomass energy system, revealed that the biomass energy system is more viable, practicable, and applicable than the complexity of the solar-based energy option. According to the findings of this manuscript by Nordic et al. [57], the biomass system

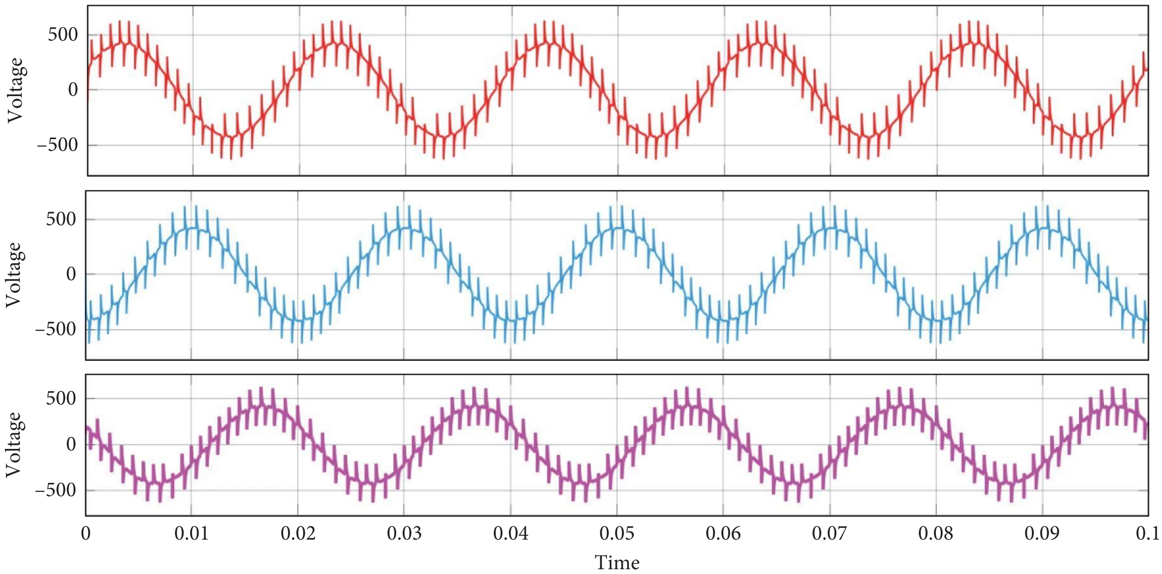

FIGURE 10: Voltage waveform during synchronization.

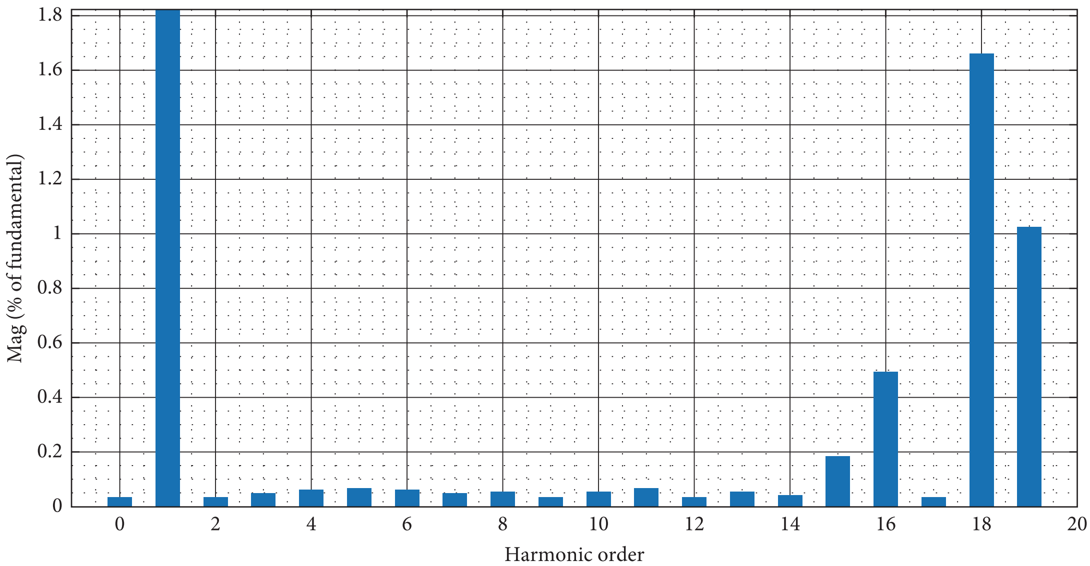

FIGURE 11: Total harmonic distortion, fundamental (50 Hz), 422.5, and THD of 4.75%. THD, total harmonic distortion.

model is flexible and easily applicable to rural-based areas for reliable power generation and harvesting compared with solar-based energy models [36, 57].

Another study based on the findings of the IEEE research output by Deshpande and Bhasme [1, 34, 37] presented different inverted model topologies with central/string and microinverter models-PV systems. The findings of this paper present these system model capabilities as noteworthy and fit for grid-connection considerations. Nordic et al. [36, 58–61] delved into the limitations of the grid-connected inverter PV system, such as THD ≤ 5%, DC current injection, and anti-islanding detection standards. Several topological dynamics for inverter-based grid-connected PV systems are addressed in this study. Moreover, Nordic et al. highlighted that multistring topology systems are highly advanced compared with both central and string or the other existing inverter models. The multistring inverter displayed high and reliable energy efficiency, coupled with a good sense of practicality and applicability standards. This study highly recommended the multistring topology for a typical grid connection, as it is highly economically viable and efficient in terms of installation and maintenance sequence costs, has high energy efficiency, and is more practical and applicable.

According to Adak and Cangi [28] solar PV energy has become a significant focus for researchers due to its rapid global adoption. Despite its numerous advantages, PV energy poses certain challenges, particularly concerning PF and THD [28]. When integrated into the grid, solar PV systems can lead

Table 6: Summary of previously performed inverter models for grid connection.

MFC inverter optimization model for grid connection						
Inverter model	**Inverter configuration**	**Costs analysis**	**Power/VAC**	**Energy efficiency**	**IEEE compliant**	**References**
Honeywell model/biomass power	1/3 phase	Cost-effective	5 MW	High	Yes	[57]
Central PV-inverter	3 phase	Cost-effective	2 kW	Average	Yes	[36]
String-multi-PV inverter	1/3 phase	Less cost-effective	2 kW	More than central inverter model	—	[36, 58]
Microinverter	1 phase	Very low-cost-effective	400 W	Higher than central and string	Yes	[7, 58]
Multilevel-inverter	3 phase	Highly cost-effective	400 VDC	Simulation stage-high	Yes	Current study

Abbreviations: MFC, microbial fuel cell; PV, photovoltaic.

to various power quality issues [28]. These issues, such as component overheating and suboptimal operation, arise mainly from low power quality and high harmonics, causing significant damage. The magnitudes of PF and THD are influenced by solar irradiation levels. This article studied how changes in solar irradiation (G) impact power quality in grid-connected solar systems, presenting and analyzing results for different irradiation conditions [28]. At low irradiance levels, the amplitude of harmonic components and reactive power increases, while the PF decreases, leading to reduced system efficiency.

The current work, addressed by this manuscript, also delves into the computational optimization and simulation of the multilevel inverter-based model toward achieving highly convincing and reliable results in terms of the THD of 4.75%, which is clearly under the limitations standards stated by Nordic et al. [3, 5, 7, 36, 57–61] (IEEE-International Standards) in the above findings as 5%. This current work underpins the convincing harmonic distortion of 422.5, moreover toward being IEEE compliant and reliable [7, 58]. Figures 8–11 clearly indicate the multilevel system findings and simulation outputs as well within the threshold limits set by the IEEE Boards of Standards. Figures 8–11 indicate reduced harmonic distortion values and a reasonable overall voltage yield of 400 VDC per 50 Hz. Conclusively, the current research highly recommends the application of the multilevel inverter model as viable for national energy grid connections because of its IEE-compliant nature and overall output. Owing to its low installation cost, this model is highly cost-effective and has a high sense of reliability, sustainability, and high energy efficiency considering its voltage output, with that magnitude of the DCMFC as a sustainable battery source of bioenergy.

4. Conclusions

In summary, Table 6 provides a comparison between previous studies on inverter modeling for practical grid connections and the outcomes of the current study. The Honeywell biomass power plant model, as reported by Norder, Min, and Logan [34], emphasizes the importance of key components such as the boiler, steam turbine, and generator in achieving a 5 MW power output, requiring approximately 8.33 tonnes/h of wood waste. This model favors biomass energy systems over solar-based options because of their practicality and applicability, particularly in rural areas.

Briefly, Adak and Cangi's [28] findings highlight the significant impact of solar irradiation on power quality in grid-connected solar PV systems. It demonstrates that low irradiance levels increase harmonic components and reactive power while decreasing the PF, leading to reduced system efficiency. By developing a MATLAB-simulated model and deriving new analytical expressions for PF and THD_I using SPSS and curve fitting methods, the study provides valuable tools for mitigating power quality issues in low irradiation scenarios. These findings offer critical insights for improving the integration of solar PV systems into the grid, enhancing their reliability and performance.

Another study by Deshpande and Bhasme [1] explored different inverter model topologies for PV systems, highlighting their suitability for grid connection. Nordic et al. further discussed the limitations and dynamics of grid-connected PV systems, favoring the multistring topology for its efficiency, practicality, and cost-effectiveness. The current research focuses on computational optimization and simulation of a multilevel inverter-based model, achieving a low THD of 4.75%, which is well below the IEEE standard of 5%. The findings demonstrate reduced harmonic distortion and satisfactory voltage yield, indicating the viability of the multilevel inverter model for national energy grid connection. Overall, the model offers low installation costs, high reliability, sustainability, and energy efficiency, making it a promising option for bioenergy storage and grid integration.

Conclusively, the utilization of a multilevel inverter configuration in this study has proven to be effective in reducing the harmonic content, as demonstrated by the sinusoidal pattern of three-phase voltages recorded at 400 V and 50 Hz. The distinct separation of waveforms at 120° intervals maintains synchronized phase sequences, enhancing the coherence between the grid and inverter voltages. Additionally, the calculated THD of 4.75% at a frequency of 50 Hz underscores the effectiveness of the multilevel inverter in minimizing harmonic distortion. This finding, supported by a harmonic distortion value of 422.5, highlights the success of the chosen configuration in achieving reduced harmonic content, thus contributing to the overall reliability and efficiency of the system.

To conclude, the computational modeling of grid-connected DCMFC bioenergy via MATLAB Simulink software has yielded novel findings. The study has provided valuable insights into the dynamic interactions of DCMFC within a grid-connected framework, offering predictions on power generation and contributing to a deeper understanding of its integration potential. Additionally, the research has addressed the compliance of the DCMFC inverter with established conventional standards and IEEE standards, further enhancing the feasibility and applicability of this bioenergy/bioelectrochemical technology (BES) in a real-world grid scenario. These novel findings advance the knowledge base in the field of renewable energy systems and pave the way for more efficient and sustainable grid-connected bioenergy solutions.

Data Availability Statement

The data that support the findings of this study are available from the corresponding author upon reasonable request.

Ethics Statement

The authors have nothing to report.

Consent

The authors have nothing to report.

Conflicts of Interest

The authors declare no conflicts of interest.

Author Contributions

Khaya Pearlman Shabangu and Nhlanhla Mthembu: conceptualization, methodology, formal analysis, investigation. **Khaya Pearlman Shabangu:** validation, data curation, writing–original draft preparation, writing–review and editing, visualization. **Babatunde Femi Bakare and Manimagalay Chetty:** resources, supervision. **Babatunde Femi Bakare:** project administration. **Babatunde Femi Bakare, Manimagalay Chetty and Khaya Pearlman Shabangu:** funding acquisition. All authors have read and agreed to the published version of the manuscript.

Funding

This manuscript received a research grant as funding from Durban University of Technology (DUT), Mangosuthu University of Technology (MUT), and Cape Peninsula University of Technology (CPUT).

Acknowledgments

K.P. Shabangu would like to extend his sincere gratitude to B. F. Bakare for his invaluable support, guidance, and patience throughout my work, as well as for proofreading the contents of this review manuscript. K.P. Shabangu is also deeply grateful to M. Chetty (Head of Department and Research Group Leader, Department of Chemical Engineering, CPUT) for his significant contributions in advising and proofreading this article. Finally, K.P. Shabangu would like to express his heartfelt appreciation to N. Mthembu for his invaluable contributions, the Departments of Research and Innovation at Mangosuthu University of Technology (MUT) and Durban University of Technology (DUT) for their generous funding of the APC costs for this article.

References

[1] S. Deshpande and N. R. Bhasme, "A Review of Topologies of Inverter for Grid Connected PV Systems," in *Power and Advanced Computing Technologies (i-PACT)*, (Vellore, India: IEEE, 2017), 1–6.

[2] H. Lund, J. Z. Thellufsen, P. A. Østergaard, P. Sorknæs, I. R. Skov, and B. V. Mathiesen, "EnergyPLAN e Advanced Analysis of Smart Energy Systems," *Smart Energy* 1 (2021): 100007.

[3] R. Tomaszewski, "A Study of Citations to STEM Databases: ACM Digital Library, Engineering Village, IEEE *Xplore*, and MathSciNet," *Scientometrics* 126 (2021): 1797–1811.

[4] Q. Zhang, X. Sun, Y. Zhong, and M. Matsui, "A Novel Topology for Solving the Partial Shading Problem in Photovoltaic Power Generation System," in *2009 IEEE 6th International Power Electronics and Motion Control Conference*, (Wuhan: IEEE, 2009), 2130–2135.

[5] "IEEE Xplore Full-Text PDF," https://ieeexplore.ieee.org/stamp/stamp.jsp?arnumber=5157752&casa_token=9rON4j_CRNEAAAAA:b7njGG4xgb2SA_YJ9EettxGRgpOYk9b-HlsxZUDg1DkbpvUqt97nJCgUlY9_CJlfoen7o9nutouGhc.

[6] Q. Zhang, X. Sun, Y. Zhong, and M. Matsui, "A novel topology for solving the partial shading problem in photovoltaic power generation system," in *2009 IEEE 6th International Power Electronics and Motion Control Conference*, (Wuhan: IEEE, 2009), 2130–2135.

[7] S. B. Kjaer, J. K. Pedersen, and F. Blaabjerg, "A Review of Single-Phase Grid-Connected Inverters for Photovoltaic Modules," *IEEE Transactions on Industry Applications* 41, no. 5 (2005): 1292–1306.

[8] "IEEE Xplore Full-Text PDF:" https://ieeexplore.ieee.org/stamp/stamp.jsp?arnumber=1510827&casa_token=fVIIkAkaiWUAAAAA:ZiLBqWi73-hKah_M44rD3UUfuloQHkXTgbQeld3hlnGhMkIpz1Pk7D2DVRaNGnrbtargic_bRnijtM.

[9] A. Lundqvist, "Future Development of Bioenergy in South Africa: A Study of Increased Use of Available Biomass for the Future Development of Renewable Energy in South Africa," (2020).

[10] H. Ren, Q. Wu, W. Gao, and W. Zhou, "Optimal Operation of a Grid-Connected Hybrid PV/Fuel Cell/Battery Energy System for Residential Applications," *Energy* 113 (2016): 702–712.

[11] W. Badenhorst, J. Zhang, and X. Xia, "Optimal Hoist Scheduling of a Deep Level Mine Twin Rock Winder System for Demand Side Management," *Electric Power Systems Research* 81, no. 5 (2011): 1088–1095.

[12] S. M. Sichilalu and X. Xia, "Optimal Energy Control of Grid Tied PV-Diesel-Battery Hybrid System Powering Heat Pump Water Heater," *Solar Energy* 115 (2015): 243–254.

[13] A. S. O. Ogunjuyigbe, T. R. Ayodele, and O. A. Akinola, "Optimal Allocation and Sizing of PV/Wind/Split-Diesel/Battery Hybrid Energy System for Minimizing Life Cycle Cost, Carbon Emission and Dump Energy of Remote Residential Building," *Applied Energy* 171 (2016): 153–171.

[14] D. J. van Vuuren, A. Marnewick, and J. H. C. Pretorius, "A Proposed Simulation-Based Theoretical Preconstruction Process: The Case of Solar Photovoltaic Technology in South African Shopping Centres," *Renewable and Sustainable Energy Reviews* 113 (2019): 109295.

[15] S. La Monaca and L. Ryan, "Solar PV Where the Sun Doesn't Shine: Estimating the Economic Impacts of Support Schemes for Residential PV With Detailed Net Demand Profiling," *Energy Policy* 108 (2017): 731–741.

[16] T. Luo, A. Xuan, Y. Wang, G. Li, J. Fang, and Z. Liu, "Energy Efficiency Evaluation and Optimization of Active Distribution Networks With Building Integrated Photovoltaic Systems," *Renewable Energy* 219 (2023): 119447.

[17] M. Obi and R. Bass, "Trends, and Challenges of Grid-Connected Photovoltaic Systems—A Review," *Renewable and Sustainable Energy Reviews* 58 (2016): 1082–1094.

[18] M. S. Thopil, R. C. Bansal, L. Zhang, and G. Sharma, "A Review of Grid Connected Distributed Generation Using Renewable Energy Sources in South Africa," *Energy Strategy Reviews* 21 (2018): 88–97.

[19] D. Mayr, E. Schmid, H. Trollip, M. Zeyringer, and J. Schmidt, "The Impact of Residential Photovoltaic Power on Electricity Sales Revenues in Cape Town, South Africa," *Utilities Policy* 36 (2015): 10–23.

[20] S. Giglmayr, A. C. Brent, P. Gauché, and H. Fechner, "Utility-Scale PV Power and Energy Supply Outlook for South Africa in 2015," *Renewable Energy* 83 (2015): 779–785.

[21] J. E. Campbell, D. B. Lobell, R. C. Genova, and C. B. Field, "The Global Potential of Bioenergy on Abandoned Agriculture Lands," *Environmental Science & Technology* 42, no. 15 (2008): 5791–5794.

[22] H. Haberl, K. H. Erb, F. Krausmann, et al., "Global Bioenergy Potentials From Agricultural Land in 2050: Sensitivity to

Climate Change, Diets, and Yields," *Biomass and Bioenergy* 35, no. 12 (2011): 4753–4769.

[23] M. Ejigu, "Toward Energy and Livelihoods Security in Africa: Smallholder Production and Processing of Bioenergy as a Strategy," *Natural Resources Forum* 32, no. 2 (2008): 152–162.

[24] B. P. Numbi and X. Xia, "Optimal Energy Control of a Crushing Process Based on Vertical Shaft Impactor," *Applied Energy* 162 (2016): 1653–1661.

[25] B. P. Numbi and S. J. Malinga, "Optimal Energy Cost and Economic Analysis of a Residential Grid-Interactive Solar PV System-Case of eThekwini Municipality in South Africa," *Applied Energy* 186 (2017): 28–45.

[26] B. Msimanga and A. B. Sebitosi, "South Africa's Non-Policy Driven Options for Renewable Energy Development," *Renewable Energy* 69 (2014): 420–427.

[27] J. Wolf, P. S. Bindraban, J. C. Luijten, and L. M. Vleeshouwers, "Exploratory Study on the Land Area Required for Global Food Supply and the Potential Global Production of Bioenergy," *Agricultural Systems* 76, no. 3 (2003): 841–861.

[28] S. Adak and H. Cangi, "The Quality Problems at Low Irradiance in the Grid-Connected Photovoltaic Systems," *Electrical Engineering* 106, no. 5 (2024): 6185–6197.

[29] Q. Ren, J. You, and J. Duan, "Optimization of Rural Electric Energy Storage System Under the Background of Echelon Utilization," *Electrical Engineering* 105, no. 1 (2023): 1–11.

[30] A. Qazi, F. Hussain, N. A. B. D. Rahim, et al., "Towards Sustainable Energy: A Systematic Review of Renewable Energy Sources, Technologies, and Public Opinions," *IEEE Access* 7 (2019): 63837–63851.

[31] M. Castilla, J. Miret, J. Matas, L. G. de Vicuña, and J. M. Guerrero, "Control Design Guidelines for Single-Phase Grid-Connected Photovoltaic Inverters With Damped Resonant Harmonic Compensators," *IEEE Transactions on Industrial Electronics* 56, no. 11 (2009): 4492–4501.

[32] A. Kusko and M. T. Thompson, *Power Quality in Electrical Systems* (McGraw-Hill, New York, 2007).

[33] S. C. Ferreira, R. B. Gonzatti, C. H. Silva, L. E. B. Da Silva, R. R. Pereira, and G. Lambert-Torres, "Adaptive Real-Time Power Measurement Based on IEEE Standard 1459-2010," *Electric Power Components and Systems [Internet]* 43, no. 11 (2015): 1307–1317.

[34] J. R. Kim, B. Min, and B. E. Logan, "Evaluation of Procedures to Acclimate a Microbial Fuel Cell for Electricity Production," *Applied Microbiology and Biotechnology* 68, no. 1 (2005): 23–30.

[35] K. P. Shabangu, B. F. Bakare, and J. K. Bwapwa, "Microbial Fuel Cells for Electrical Energy: Outlook on Scaling-Up and Application Possibilities Towards South African Energy Grid," *Sustainability [Internet]* 14, no. 21 (2022): 14268.

[36] N. Gure, A. Yildiz, and A. Kukner, "Preliminary Feasibility Study on Energy Economy of Electric-Bus Rapid Transit System," in *2021 International Conference on Electrical, Computer and Energy Technologies (ICECET)*, (IEEE, 2021).

[37] K. P. Shabangu, N. Mthembu, M. Chetty, and B. F. Bakare, "Validation of RSM Predicted Optimum Scaling-Up Factors for Generating Electricity in a DCMFC: MATLAB Design and Simulation Model," *Fermentation* 9, no. 9 (2023): 856.

[38] K. P. Shabangu, B. F. Bakare, and J. K. Bwapwa, "The Treatment Effect of Chemical Coagulation Process in South African Brewery Wastewater: Comparison of Polyamine and Aluminum-Chlorohydrate Coagulants," *Water* 14, no. 16 (2022): 2495.

[39] S. Cheng, H. Liu, and B. E. Logan, "Increased Performance of Single-Chamber Microbial Fuel Cells Using an Improved Cathode Structure," *Electrochemistry Communications* 8, no. 3 (2006): 489–494.

[40] B. E. Logan, B. Hamelers, R. Rozendal, et al., "Microbial Fuel Cells: Methodology and Technology," *Environmental Science & Technology* 40, no. 17 (2006): 5181–5192.

[41] S. Cheng, H. Liu, and B. E. Logan, "Increased Power Generation in a Continuous Flow MFC With Advective Flow Through the Porous Anode and Reduced Electrode Spacing," *Environmental Science & Technology* 40, no. 7 (2006): 2426–2432.

[42] Y. Ahn, M. C. Hatzell, F. Zhang, and B. E. Logan, "Different Electrode Configurations to Optimize Performance of Multi-Electrode Microbial Fuel Cells for Generating Power or Treating Domestic Wastewater," *Journal of Power Sources* 249 (2014): 440–445.

[43] B. E. Logan and K. Rabaey, "Conversion of Wastes Into Bioelectricity and Chemicals by Using Microbial Electrochemical Technologies," *Science* 337, no. 6095 (2012): 686–690.

[44] B. Min and B. E. Logan, "Continuous Electricity Generation from Domestic Wastewater and Organic Substrates in a Flat Plate Microbial Fuel Cell," *Environmental Science & Technology* 38, no. 21 (2004): 5809–5814.

[45] Y. Ahn and B. E. Logan, "Effectiveness of Domestic Wastewater Treatment Using Microbial Fuel Cells at Ambient and Mesophilic Temperatures," *Bioresource Technology* 101, no. 2 (2010): 469–475.

[46] B. E. Logan and J. M. Regan, "Electricity-Producing Bacterial Communities in Microbial Fuel Cells," *Trends in Microbiology* 14, no. 12 (2006): 512–518.

[47] R. Rossi, X. Wang, and B. E. Logan, "High Performance Flow through Microbial Fuel Cells With Anion Exchange Membrane," *Journal of Power Sources* 475 (2020): 228633.

[48] L. Ren, Y. Ahn, and B. E. Logan, "A Two-Stage Microbial Fuel Cell and Anaerobic Fluidized Bed Membrane Bioreactor (MFC-AFMBR) System for Effective Domestic Wastewater Treatment," *Environmental Science & Technology* 48, no. 7 (2014): 4199–4206.

[49] Y. Zuo, P.-C. Maness, and B. E. Logan, "Electricity Production From Steam-Exploded Corn Stover Biomass," *Energy & Fuels* 20, no. 4 (2006): 1716–1721.

[50] D. Ucar, Y. Zhang, and I. Angelidaki, "An Overview of Electron Acceptors in Microbial Fuel Cells. An Overview of Electron Acceptors in Microbial Fuel Cells," *Frontiers in Microbiology* 8 (2017).

[51] L. Zhang, J. Li, X. Zhu, D. Ye, Q. Fu, and Q. Liao, "Startup Performance and Anodic Biofilm Distribution in Continuous-Flow Microbial Fuel Cells With Serpentine Flow Fields: Effects of External Resistance," *Industrial & Engineering Chemistry Research* 56, no. 14 (2017): 3767–3774.

[52] K. P. Shabangu, N. Mthembu, M. Chetty, J. K. Bwapwa, and B. F. Bakare, "A Comparative Analysis of Organic Substrates From Industrial Wastewater Streams for Enhanced Electricity Production Using a Double Chamber Microbial Fuel Cell (DCMFC)," *Energy Reports* 11 (2024): 3050–4847.

[53] K. P. Shabangu, M. Chetty, and B. F. Bakare, "Optimization and Modelling of a Dual-Chamber Microbial Fuel Cell (DCMFC) for Industrial Wastewater Treatment: A Box-Behnken Design Approach," *Energies* 17, no. 11 (2024): 2740.

[54] A. Nayak and B. Bhushan, "Microbial Fuel Cell Technology for Bio-Electrochemical Conversion of Waste to Energy," in *Advanced Technology for the Conversion of Waste into Fuels and Chemicals*

[55] B. Xiao, F. Yang, and J. Liu, "Enhancing Simultaneous Electricity Production and Reduction of Sewage Sludge in Two-Chamber MFC by Aerobic Sludge Digestion and Sludge Pretreatments," *Journal of Hazardous Materials* 189, no. 1-2 (2011): 444–449.

[56] B. Zhang, H. Zhao, S. Zhou, C. Shi, C. Wang, and J. Ni, "A Novel UASB-MFC-BAF Integrated System for High Strength Molasses Wastewater Treatment and Bioelectricity Generation," *Bioresource Technology* 100, no. 23 (2009): 5687–5693.

[57] S. T. Nesaratnam, ed., *Water Pollution Control* (John Wiley & Sons, 2014).

[58] A. M. Nasrabadi and M. Moghimi, "Sustainable Energy Technologies and Assessments 53, 2022, 102742 4E Analysis of Stacked Microbial Fuel Cell as a Component in Power Plants for Power Generation and Water Treatment; With a Cost-Benefit Perspective," *Sustainable Energy Technologies and Assessments* 53 (2022): 102742.

[59] Lab-resisprod, "Proceeding International Conference and Workshop on Chemical Engineeringng," (2013).

[60] C. Varrone, I. V. Skiadas, and H. N. Gavala, "Effect of Hydraulic Retention Time on the Modelling and Optimization of Joint 1,3 PDO and BuA Production From 2G Glycerol in a Chemostat Process," 2018, https://www.elsevier.com/locate/cej.

[61] R. Faranda, A. Pievatolo, and E. Tironi, "Load Shedding: A New Proposal," *IEEE Transactions on Power Systems* 22, no. 4.